Computers and Concrete, *Vol. 14, No. 4 (2014) 369-385*
DOI: http://dx.doi.org/10.12989/cac.2014.14.4.369

Numerical analysis for behavior of outer concrete tank in emergency LNG spillage

Jeong Su Lee[1a], Chan Kyu Park[2b], Yun Lee[3c], Ji-Hoon Kim[4d] and Seung Hee Kwon[*]

[1]*Department of Civil and Environmental Engineering, Myongji University, Yongin, 449-728, Republic of Korea*
[2]*Construction Technology Research Institute, Samsung C&T Corporation, Seocho-Gu, Seoul, 137-857, Republic of Korea*
[3]*Department of Civil Engineering, Daejeon University, Daejeon, 300-716, Republic of Korea*
[4]*Energy System Team, Samsung C&T Corporation, Seocho-Gu, Seoul, 137-956, Republic of Korea*

(*Received December 9, 2013, Revised August 11, 2014, Accepted August 20, 2014*)

Abstract. In the existing method for analyzing the liquid tightness of the outer concrete tank in an emergency LNG spillage, the temperature variation over time inside the tank, and the concrete properties dependent on temperature and internal moisture content, have not been taken into account. In this study, the analyses for a typical LNG concrete tank subjected to thermal load due to spillage were performed with three different cases: the existing method was adopted in the first case, the transient temperature variation was considered in the second, and the temperature-moisture content dependent concrete properties were taken into account as well as the transient states of temperature in the third. The analysis results for deformation, compressive zone size, cracking, and stress of reinforcements were compared, and a discussion on the difference between the results obtained from the different analysis cases was made.

Keywords: LNG; spillage, liquid tightness; crack, compression zone

1. Introduction

In the process of designing a LNG storage tank, it is mandatory to examine whether the outer concrete tank satisfies the criteria for liquid tightness in the event of emergency LNG spillage. The compressive zone size of concrete (10% of the wall and in no case less than 80 mm), the average stress in the compressive zone (greater than 1 MPa), the stress level of reinforcements (less than yield stress), and the surface crack widths at the thermal corner protection (less than 0.3 mm) are mainly investigated by a numerical analysis of the outer concrete tank subjected to thermal shock (ACI373 1997, BS 7777 1993, PCI 1987, prEN 265002 2001, prEN 14620 2003).

In the existing method of numerical analysis for estimating liquid tightness, which has been

∗Corresponding author, Associate professor, E-mail: kwon08@mju.ac.kr
[a]Graduate student, E-mail: jung86ss@gmail.com
[b]Principal research engineer, E-mail: helpme@samsung.com
[c]Assistant professor, E-mail: yunis@dju.ac.kr
[d]General Manager, E-mail: jason66.kim@samsung.com

http://www.techno-press.org/?journal=cac&subpage=8 ISSN: 1598-8198 (Print), 1598-818X (Online)

widely adopted in practice, a thermal analysis is first performed under the assumption that LNG of -168℃ is in direct contact with the inner wall of the concrete tank, and the temperature profile inside the wall is in equilibrium, namely, in the steady state. In sequence, based on the temperature profile inside the tank in the steady state, the structural analysis for stress, strain and cracking follow.

It is most likely impossible to verify if the results of the analysis will be in good agreement with the actual behavior of the outer tank in an actual spillage because an emergency spillage similar to the conditions considered in the analysis has never happened so far. Therefore, in order to ascertain the realistic behavior of the outer tank in a spillage, the actual phenomena induced by the abrupt temperature change needs to precisely considered in the analysis. However, there are two aspects which are considered differently from the actual phenomena in the existing analysis method.

In reality, it would take some time, probably several days, for the temperature to reach a steady state after the spillage. By not reflecting the transient states of the temperature the analysis may not give an accurate estimation of the liquid tightness (Rötzer and Douglas 2006, Lee 2006, Jeon *et al*. 2007, Lee *et al*. 2009, Gorla 2010, Gillard *et al*. 2012). In addition, although the mechanical properties of concrete highly depend on temperature and the internal moisture content, it is assumed in the existing analysis method that the constitutive law for the concrete material is independent of the temperature or the internal moisture content.

The objective of this study is to elaborate an analysis method for the outer concrete tank in a spillage by taking the aforementioned two aspects into account. A LNG concrete tank of a typical shape and dimensions was selected, and spillage analyses for the selected tank were performed for three different cases. In the first case, the existing analysis method was adopted. In the second, the transient state of the internal temperature was taken into account in the analysis. In the third, the materials properties of concrete with varying temperature and internal moisture content as well as the transient temperature were simultaneously considered. Analysis results for the deformation, cracking, compressive zone, and stress of reinforcements were determined, and a discussion on the difference between the results obtained from the different analysis cases was made.

2. Mechanical properties of concrete in cryogenic temperature

Many researchers (Bamforth *et al*. 1983, Dahmani *et al*. 2007, Goto and Miura 1979, Jeon 2004, Jo *et al*. 2009, Marshall 1982, Marechal, 1972, Miura 1989, Kogbara *et al*. 2013, Krstulovic-Opara 2007, Rostasy and Wiedemann 1980) have studied the various physical properties of concrete at cryogenic temperatures, such as thermal conductivity, permeability, thermal strain (expansion coefficient), elastic modulus, tensile and compressive strengths, etc. The temperature-dependent properties considered in this study are summarized herein.

The compressive strength of concrete generally increases with the decrease of temperature, but this tendency is greatly influenced by the internal moisture content because of the moisture freezing. The compressive strength can be simply expressed as follows:

$$f_c' = f_{c0}' + \Delta f_c' \tag{1}$$

where f_c' (MPa) is the compressive strength of concrete, f_{c0}' (MPa) is the compressive strength at normal temperature (around 20℃), and f_c' (MPa) is the increment according to the variation of

the temperature and the moisture content, for which the following empirical model was previously zzsuggested by Miura (1989):

$$\Delta f_c' = \left[12.2 - \frac{1}{2646}(T+180)^2 \right] w \quad (T \geq -120^{\circ}\mathrm{C}) \tag{2}$$

$$\Delta f_c' = 10.9w \quad (T < -120^{\circ}\mathrm{C}) \tag{3}$$

where T is the temperature (℃) and w is the moisture content(%). Several experimental studies were previously performed to examine tensile strength at low temperature (Goto and Miura 1978, Okada and Iguro 1978), and a correlation of the tensile strength with the compressive strength were made by Goto and Miura (1979) as follows:

$$f_t = 0.215(f_c')^{0.75} \tag{4}$$

where f_t is the tensile strength (MPa). The elastic modulus at low temperature can be also correlated with the compressive strength, and several models have been suggested (Monfore and Lentz 1962, Yamane *et al*. 1978). However, more experimental verification is needed to confirm any of these models, and a model suggested in the design specification (BS 8110-1 1997) was used in this study. The elastic modulus was considered as a function of the compressive strength:

$$E_0 = 5.5\sqrt{f_c'} \tag{5}$$

where, E_0 is the elastic modulus of concrete (GPa) (BS 8110-1 1997).

As for Poisson's ratio, it was reported that it remains almost constant for wet concrete over the temperature range of 24℃ to -157°C. It was also observed that Poisson's ratio for concrete in equilibrium with the atmospheric relative humidity of 50% is lower than Poisson's ratio for dried concrete. It is difficult to decide a specific value or a function of Poisson's ratio over the range of normal to cryogenic temperature because the results of the existing studies are controversial. Therefore, a constant value of Poisson's ratio suggested in the design specification was adopted in this study.

3. Numerical analysis for outer concrete tank in the spillage

3.1 General

Fig. 1 shows the outer concrete tank of a typical shape and dimension, which was selected for the liquid tightness analysis in this study. Commercial finite element programs which have been broadly verified in research and practice are usually requested for use in analysis for spillage by clients for LNG storage facilities. One of the commercial codes, ADINA (2011), was used in this study.

The steel liner of 5 mm thickness is installed over the inner surface of the outer concrete tank for the gas tightness. However, the effect of the liner on the liquid tightness is generally not considered in the process of designing a LNG tank. The layer thickness is very thin and the ignorance of the liner gives a conservative result in the design. The liner is also not taken into account in this study and there is no criterion on the liner for the liquid tightness.

In the modeling, the boundary condition was assumed to be close to the real structure as much

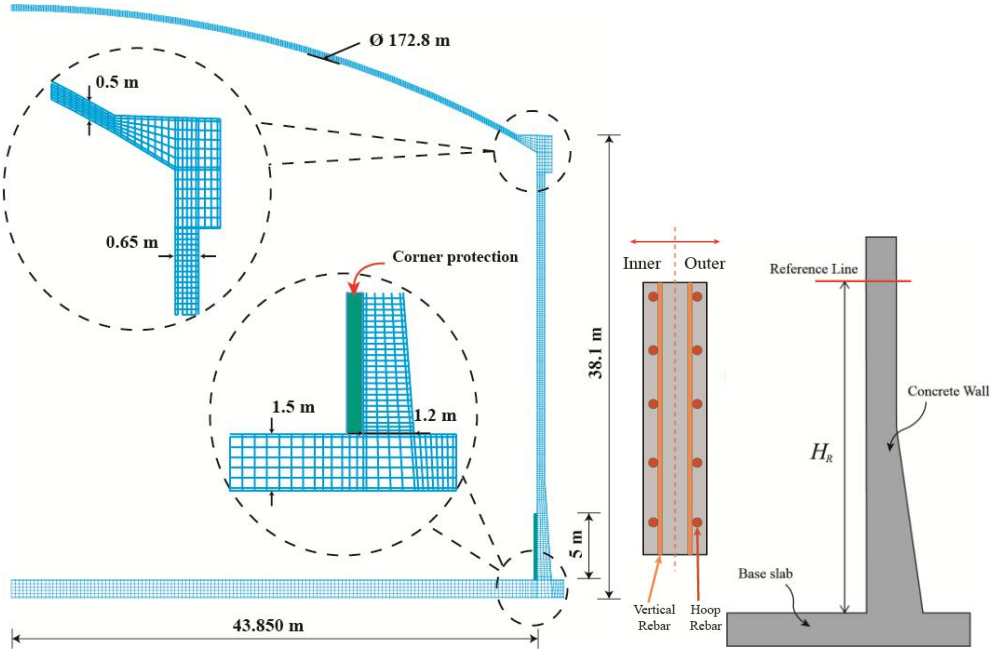

Fig. 1 Dimension and mesh refinement of outer concrete tank

as possible because it may greatly affects the structural behavior. The vertical displacement at the bottom of the concrete slab was restrained. However, elastic spring elements that have stiffness only in the horizontal direction were located at the bottom of the concrete slab considering the seismic isolators installed between the bottom slab and the piles. The lateral deformation at the center line, namely, the symmetric axis, was retrained, but the vertical deformation at the center line was allowed.

The analyses for three different cases were performed. In the first case, Case 1, only the steady state of the internal temperature profile in the concrete tank was considered, and the properties of concrete at normal temperature were applied to the entire range of temperatures, even to the cryogenic temperature. This is the analysis method which has been widely adopted in design practice.

In the second case, Case 2, the material properties were the same as Case 1, and the variation of the internal temperature over time after spillage was taken into account. In the third case, Case 3, the mechanical properties of concrete depending on temperature and internal moisture content as well as the transient temperature were simultaneously considered. In Case 1 and Case 2, the time period from the beginning of the spillage to the steady state or the equilibrium in the temperature distribution inside the tank were divided into several steps, and at each step the structural analysis was carried out based on the corresponding temperature distribution.

3.2 Modeling

A two dimensional axisymmetric model was adopted, as shown in Fig. 1, and eight node plane elements were used for modeling concrete. LNG of -168℃ was assumed to be directly in contact with the lateral surface of the wall and with the top surface of the insulating materials over the

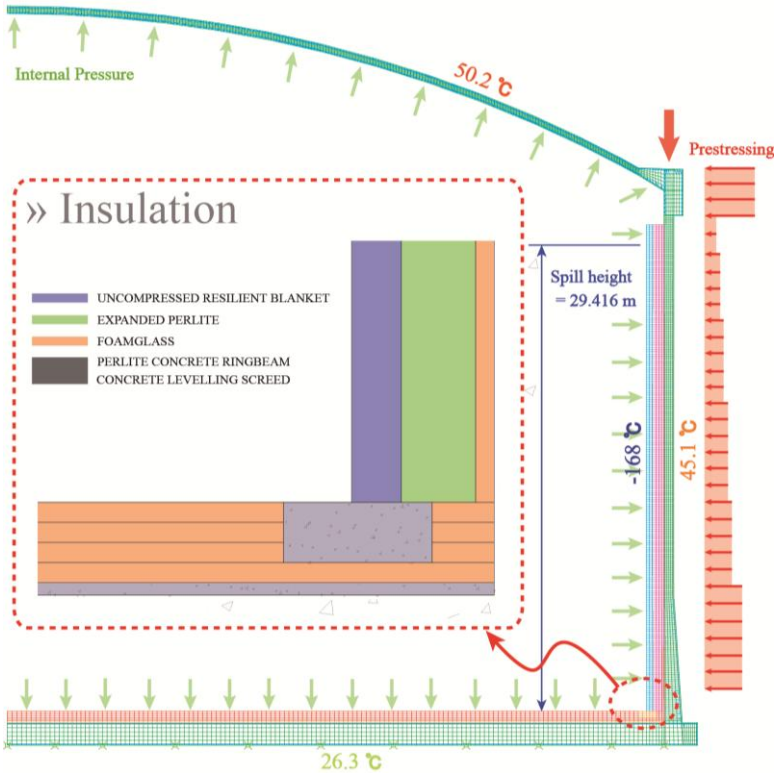

Fig. 2 External loads and temperatures imposed on the tank

Table 1 Lateral pressure corresponding to hoop pre-stressing force

Change height above top of base (m)	Hoop prestress (kN/m^2)
0 (Top of base)	0
3.775	0 234.8
7.425	234.8 166.4
12.975	166.4 140.8
16.925	140.8 122.0
19.975	122.0 107.7
22.575	107.7 96.3
26.450	96.3 99.8
33.400 (Underside of ring beam)	99.8 285.9
36.600 (Top of the wall)	285.9

bottom slab. The 5.0 m long thermal corner protection, which was made of 9% nickel steel and located in the longitudinal direction of the wall from the bottom corner, was considered in the modeling. The temperatures of the ground facing to the slab, outside of the roof, and outside of the wall were set to 26.3℃, 50.2℃ and 45.1℃, respectively, as shown in Fig. 2. The temperatures were assumed for the summer season, which may give more conservative thermal loads than the winter season.

The internal pressures due to gravity of the LNG (29 kPa), hydrostatic pressure of the spilled LNG, gas pressure (140 kPa), and compaction of the insulating material (0.46 kPa) at the lateral side of the wall were considered. The hydrostatic pressure of the spilled LNG is varying along the height of the wall, from 0.136 MPa at the base to the 0 MPa at the top of the spillage.The prestressing force applied to the wall in the vertical direction was equivalent to the stress of 1.8 MPa acting over the wall width. In order to simulate the prestressing force applied in the circumferential direction in 2D-axisymmetric modeling, the equivalent lateral stresses acting over the outside surface of the wall were imposed as shown in Fig. 2, and the values of the stresses according to height are listed in Table 1. The variation and magnitude of the hoop pre-stress along the height of the wall is determined to compensate the hydrostatic pressure of the spilled LNG.

The reinforcements placed in the vertical and horizontal directions were also modeled with a line element, namely, embedment element, and the reinforcement in the circumferential direction was modeled as a special point element provided by the program, ADINA.

3.3 Material models

In the scheme of the analysis for the spillage, the heat transfer was first calculated, and the structural analysis then followed based on the result of the calculated temperature profiles. The insulating materials located over the bottom slab were only considered in the heat transfer analysis and not regarded as a structural member. The specific heat of the formglass, perlite, and resilient blanket are 0.76, 0.39, and 0.79 kJ/kg℃, respectively. Table 2 gives the conductivities of the insulating materials.

The thermal and structural properties of the reinforcement are summarized in Table 3. A perfect elasto-plastic model was used for the mechanical behavior of the reinforcements. As for the concrete, a model provided by ADINA was adopted; the details of the model are given in the literatures (ADINA 2011, Bathe *et al*. 1989, Khatri and Anderson 1995). The multi-axial damage and plasticity in compression and the cracking in tension can be simulated. The parameters representing the stress-strain relationship in uniaxial loading, as depicted in Fig. 3, were used as inputs of the concrete model, and the damage, plasticity, failure and tensile cracking were calculated based on those parameters. Table 4 gives the thermal and mechanical parameters of concrete used in the analysis. In the finite element modeling, concrete cracking was modeled as the smeared crack model (Kwon *et al*. 2007, Kwon and Shah 2008), in which crack width is transformed into the cracking strain of the continuum body by dividing the displacement by the element size so as to impose the same facture energy to each element.

The ultimate strain in tension was set to the value equivalent to a crack opening of 0.1 mm.

In the analysis Case 3, to consider the temperature and moisture dependency of the mechanical properties of the concrete, it's necessary to estimate the internal moisture content of the concrete. A nonlinear moisture diffusion analysis was additionally performed to find the distribution of the relative humidity (RH) inside the tank. The internal moisture was assumed to diffuse toward the

Table 2 Thermal conductivities of foamglass, perlite, and resilient blanket

Temperature (°C)	Thermal conductivity (W/m°C)		
	foamglass	perlite	resilient blanket
40	0.0479	0.056	0.059
20	0.0446	0.051	0.054
0	0.0414	0.047	0.050
-20	0.0388	0.044	0.046
-40	0.0358	0.041	0.042
-80	0.0314	0.035	0.034
-120	0.0281	0.029	0.026
-160	0.0252	0.023	0.020

Table 3 Properties of reinforcement

Thermal expansion (1/°C)	0.00001
Thermal conductivity (W/m°C)	2.0
Specific heat(J/kg°C)	820
Poisson's ratio	0.3
Elastic modulus (GPa)	200
Yield strength (MPa)	415

Table 4 Properties of concrete at normal temperature

Thermal expansion (1/°C)	0.00001
Thermal conductivity	2.0 W/m℃
Specific heat	820 J/kg℃
Poisson's ratio	0.18
Elastic modulus, E_c (GPa)	41.6
Compressive strength, f_c' (MPa)	38.3
Tensile strength, f_t (MPa)	2.79
Strain at compressive strength, ε_c	1810×10^{-6}
Ultimate strain in compression, ε_u	3500×10^{-6}
Ultimate strain in tension, ε_{tu}	600×10^{-6}
Density(kg/m^3)	2500

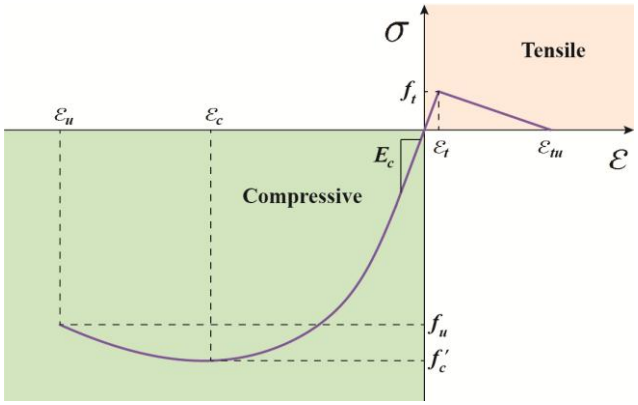

Fig. 3 Relationship between stress and strain in uniaxial loading

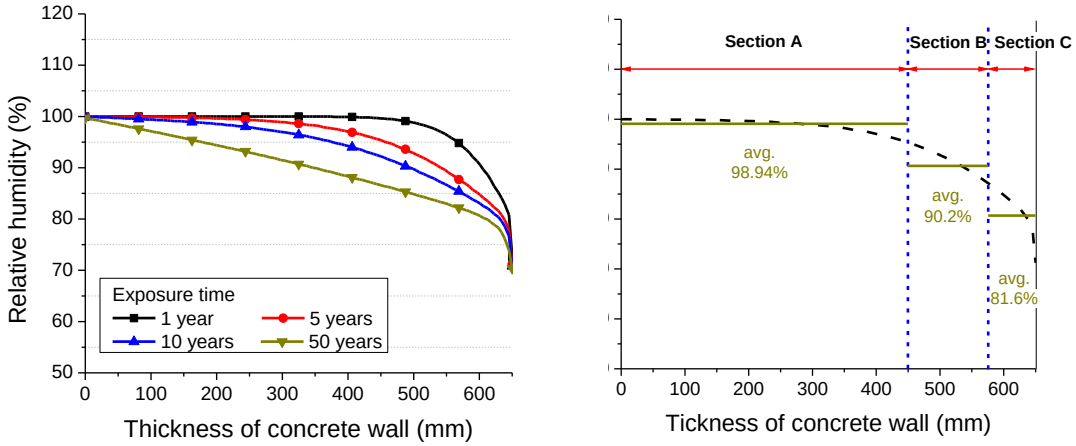

(a) Variation of RH over time (b) Simplified RH distribution at 5 years

Fig. 4 Internal relative humidity distributions over wall thickness

outside surface of the tank because evaporation of the moisture at the inside surface is prevented by the insulating and lining material. The theory and analysis method for the diffusion analysis reference existing studies (Kwon *et al*. 2007, Kwon and Shah 2008). Fig. 4(a) shows the variation of the relative humidity inside the wall over time, and the results at 5 years after construction was reflected in the analysis. The moisture diffusion highly depends on the relative humidity itself. Once the relative humidity at the surface of concrete is reduced, the moisture diffusion rate drastically decreases (Jang, Sohn, and Kwon, 2013). The relative humidity distribution of the wall at 5 years after construction is almost identical to the results at several decades after construction. In other words, the results at 5 years would represent the relative humidity distribution during the service life of the LNG tank. The cross section of the tank was divided into three parts (Section A, B, and C) as shown in Fig. 4(b), and each section was assumed to have an averaged constant relative humidity. Fig. 5(a) is the continuous distribution of the relative humidity inside the wall, and Fig. 5(b) is the simplified relative humidity distribution in the modeling.

The averaged relative humidity was transformed into moisture content based on the previously suggested method (Strube 2000), and the compressive strength, the tensile strength and the elastic modulus were calculated with the method described in Chapter 2. Table 5 shows the mechanical properties varying over temperature and moisture content, which can be considered in the concrete model provided by ADINA. In the concrete model applied to the whole structure, the variation of the mechanical properties over the range of normal to cryogenic temperature (from 50.2 ℃ to -168 ℃) was much more refined than what was shown in Table 5.

4. Results and discussions

4.1 Temperature

The temperature of -168°C was imposed on the inner surface of the wall in the analysis, and the temperature gradient was induced due to the difference between the temperatures of the inner and the outer surfaces. Fig. 6 shows the results of the thermal analysis. Fig. 6(a) is the temperature

contour in the steady state, and Fig. 6(b) and (c) are the temperature profiles over the cross section of the wall or the reference line indicated in Fig. 6(a). In the steady state, the temperature was linearly distributed as shown in Fig. 6(b). On the other hand, in the transient state, the temperature profile was nonlinearly distributed at the beginning of the spillage, becoming straight as time went by, and finally approached the steady state around 5 days after the spillage. Based on these results, the structural analyses were performed.

4.2 Deformation

The concrete tank deformed due to the temperature gradient of Fig. 6. Fig. 7(a) shows the deformed shape of the tank, magnified 250 times. The black line is for the steady state (Case 1), and the other colors are for the transient state (Case 2). As for the transient state, the deformation becomes larger with the increase of time. The maximum lateral deformation, D_{max}, of Fig. 7(b) was summarized for the three analysis cases in Table 6. The final deformations obtained from the analyses (Case 2 and Case 3) considering the temperature variation in the transient states were 12% larger than that for the steady state (Case 1). The deformations for Case 1 and Case 2 were almost identical to each other.

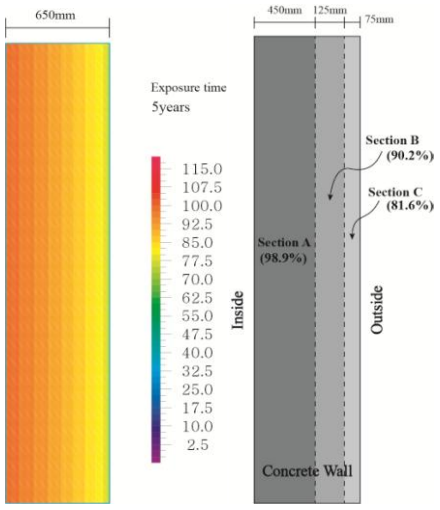

(a) RH distribution over the wall thickness (b) Simplified RH distribution for the analysis

Fig. 5 Internal relative humidity distributions at 5 years after construction

Table 5 Mechanical properties specified to the three sections of the wall

	Section A			Section B			Section C		
RH (%)	98.9			90.2			81.6		
Moisture content (%)	5.34			3.28			2.27		
Temp. (℃)	26.3	-90	-168	26.3	-90	-168	26.3	-90	-168
f'_c (MPa)	-38.26	-70.43	-76.48	-38.26	-56.71	-60.18	-38.26	-51.02	-53.42
E_c (GPa)	41.56	56.39	58.76	41.56	50.60	52.13	41.56	48.00	49.11
f_t (MPa)	2.79	3.78	3.94	2.79	3.39	3.50	2.79	3.22	3.29

4.3 Cracking

In the smeared crack model, the crack width is transformed into the tensile strain as mentioned in the above. Conversely, the crack width corresponding to the tensile strain obtained from the finite element analysis can be found. The tensile strain corresponding to the crack width of 0.3 mm was calculated, and cracks having a width larger than 0.3 mm are plotted in Fig. 8.

The crack spacing and width were larger in the steady state than those in the transient state. However, there was no crack near the corner protection, which is one of the provisions that should be fulfilled to ensure liquid tightness. The number of cracks became larger in the order of Case 1, Case 2, and Case 3. At the beginning of the transient temperature state, the temperature gradient was steeper near the inside of the wall than in the steady state. The initially steeper gradient therefore seems to induce the larger number of cracks, and the cracks propagate until the temperature distribution reaches the steady state. The larger deformation found in the analysis for Case 2 and Case 3 in Table 6, may be due to the larger number of cracks, compared to Case 1. The number of cracks larger than 0.3 mm was also listed in Table 6.

Compared to Case 2, the number of cracks is slightly increased in Case 3. As explained in Table 5, in Case 3 it was considered that the outer region of the wall had lower stiffness because of the moisture evaporation in that region. The lower stiffness leads to the increased number of cracks in Case 3.

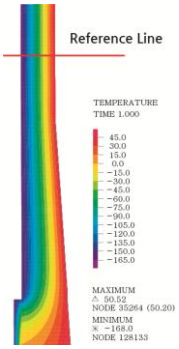

(a) Distribution of temperature in the steady state (°C)

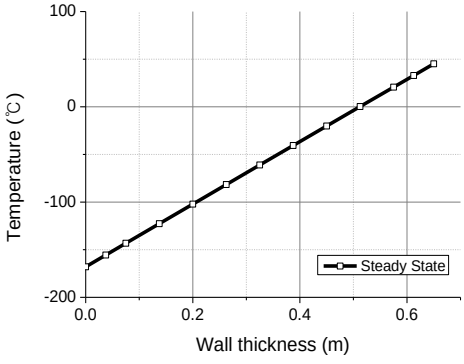

(b) Steady stat

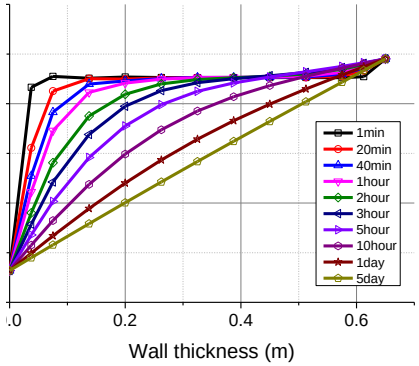

(c) Transient states

Fig. 6 Thermal analysis results

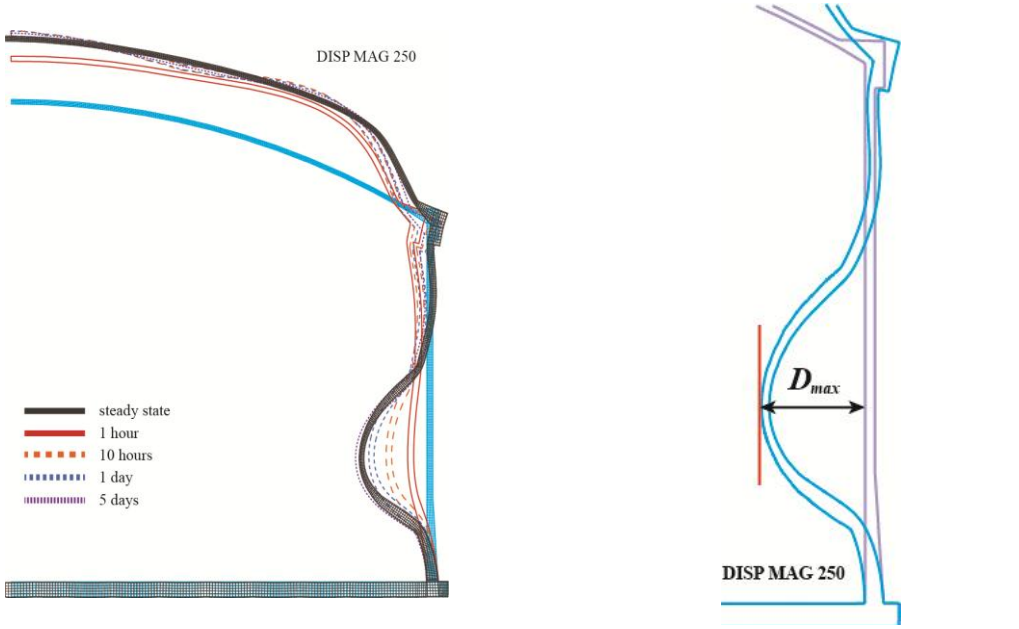

(a) Deformed shapes in the steady and transient states

(b) Maximum displacement of the wall

Fig. 7 Deformed shapes

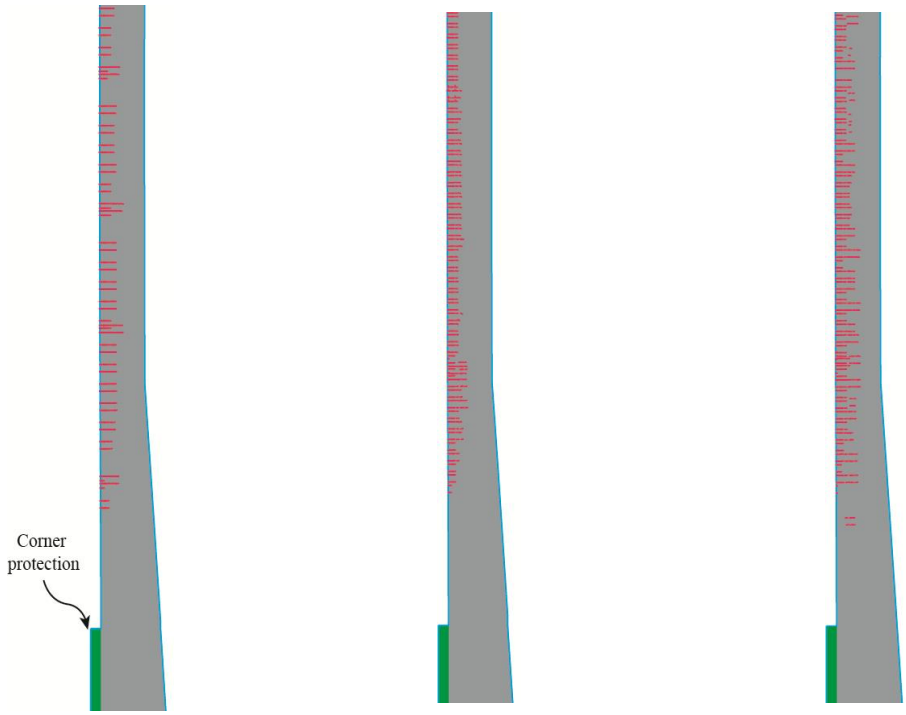

(a) Case 1 (b) Case 2 (c) Case 3

Fig. 8 Distribution of cracks larger than 0.3 mm

Table 6 Maximum displacement of the wall

Elapsed time after spillage	Maximum displacement, D_{max} (mm)			Number of cracks (larger than 0.3 mm)		
	Case 1	Case 2	Case 3	Case 1	Case 2	Case 3
1 hour		4.86	4.48		3	66
10 hours	19.53	11.41	10.45	86	151	158
1 day	(steady state)	17.41	16.59	(steady state)	147	155
5 days		21.92	21.87		149	161

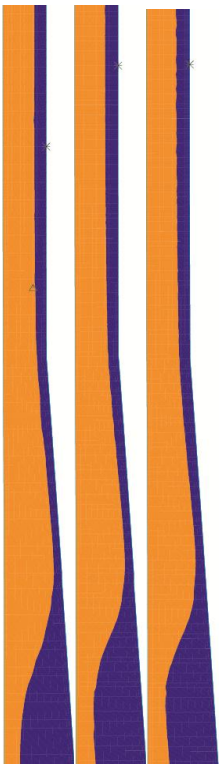

(a) Case 1 (b) Case 2 (c) Case 3

Fig. 9 Stress of concrete in hoop direction (MPa

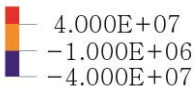

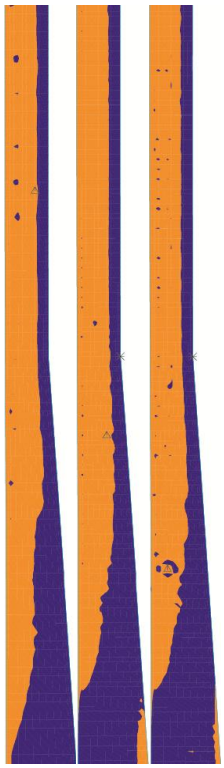

(a) Case 1 (b) Case 2 (c) Case 3

Fig.10 Stress of concrete vertical direction.(MPa)

4.4 Compressive zone of concrete

The minimum size of the compressive zone and the average stress at the minimum compressive zone are two of the key factors for estimating the liquid tightness. The contours of the concrete stresses in the hoop direction and in the vertical direction are displayed in Figs. 9 and 10, in which the blue part is the compressive zone with more than 1 MPa in compression. It can be seen that the stress contours slightly change according to the analysis cases. The stress profiles over the cross section at the minimum compressive zone are plotted in Fig. 11. The size of the zone and the average stress over the compressive zone are listed in Table 7. The positions in height for the minimum compressive zones of the hoop and the vertical stresses were different according to the analysis cases, and are also listed in Table 7. The average stress of the minimum compressive

Table 7 Position in height, size and average stress of compression zone

Analysis	Compression zone					
	Hoop direction			Vertical direction		
	Position in height H_R (m)	Size (mm)	Average (MPa)	Position in height H_R (m)	Size (mm)	Average (MPa)
Case 1	29.8	120.0	-7.7	26.8	175.0	-12.6
Case 2	6.8	145.8	-5.5	19.7	174.7	-11.5
Case 3	30.2	132.2	-9.4	9.9	177.9	-14.8

zones was the highest in the Case 3, and the smallest in the Case 2. The size of the minimum compressive zone for the vertical stress was very similar to one another, and the size for the hoop stress became wider in the Case 2 and Case 3.

4.5 Stress of reinforcements

The stresses of the reinforcements placed in the hoop and the vertical directions are plotted over the height of the wall in Figs. 12 and 13. Although the stresses for Case 2 and Case 3 are slightly lower than those for Case 1, the difference between the stress profiles for the three analysis cases are meaninglessly small. The maximum and minimum stresses for all the cases were listed in Table 8, from which all the stresses were less than the yield stress (415 MPa).

The reinforcements located at the inner side of the wall are subjected to high tensile stress caused by thermal contraction at very low temperature, while the reinforcements at the outer side are in compression. The shape of the stress profiles are very similar to the deformed shape of the wall illustrated in Fig. 7. However, the stress level in tension is much higher than that in compression. The reinforcements located in the inner part of the wall bear almost the entire amount of the tension force because of cracking, while the reinforcements and the concrete are subjected to the compression force together in the outer part of the wall. This is the reason for the higher level of stress in the tension region.

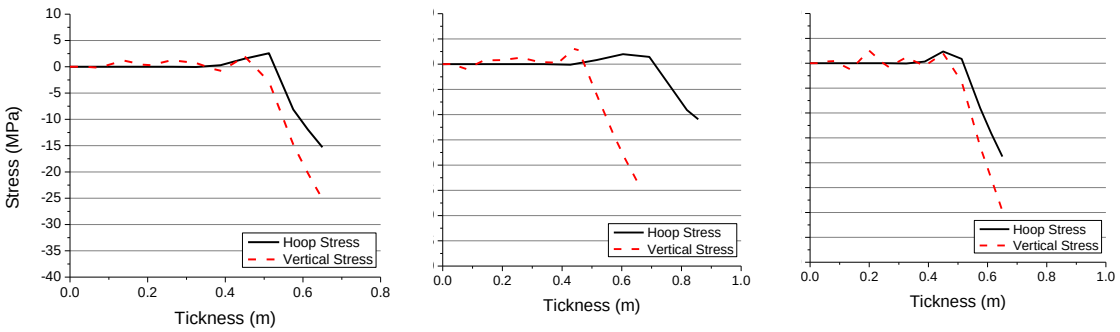

(a) Case 1 (b) Case 2 (c) Case 3

Fig.11 Stress profile over the cross section of the wall where the compression zone is the smallest

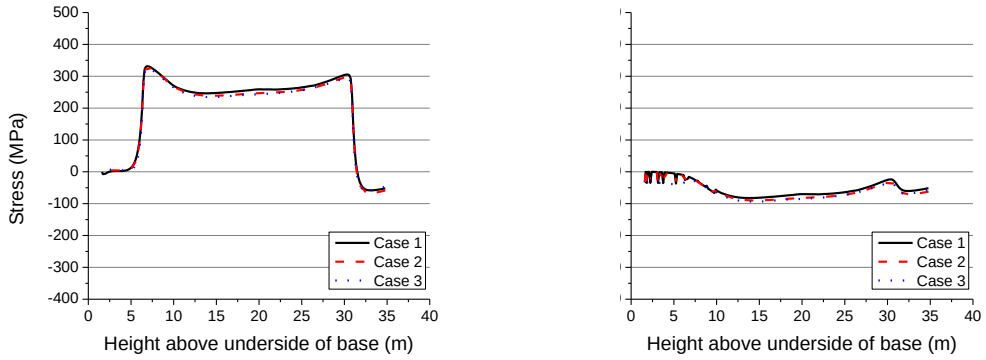

(a) Inner side of the wall (b) Outer side of the wall

Fig.12 Stresses of reinforcement placed in hoop direction

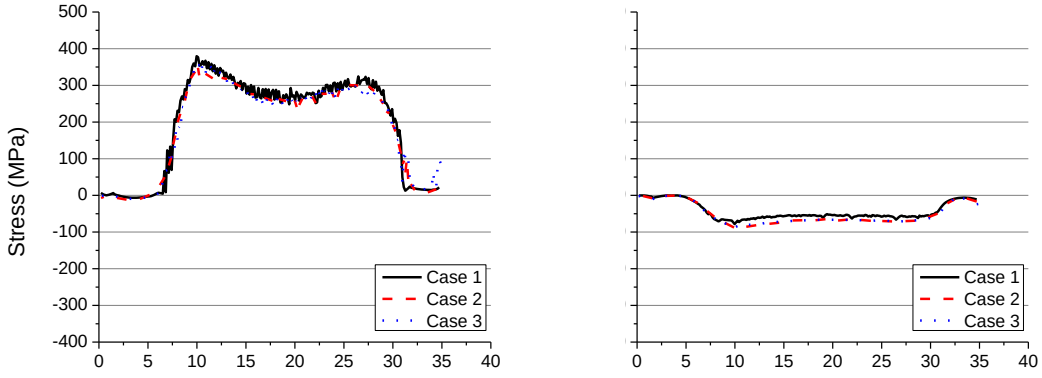

(a) Inner side of the wall (b) Outer side of the wall

Fig.13 Stresses of reinforcement placed in vertical direction

Table 8 Maximum and minimum stress of reinforcement in the wall

Anlaysis	Hoop – Inner side		Hoop – Outer side		Vertical – Inner side		Vertical – Outer side	
	Max (MPa)	Min (MPa)	Max (MPa)	Min (MPa)	Max (MPa)	Min (MPa)	Max (MPa)	Min (MPa)
Case 1	331.6	-58.2	-0.03	-82.3	379.7	-6.50	-0.03	-78.4
Case 2	329.9	-66.5	-0.39	-90.0	350.7	-12.3	-0.25	-89.6
Case 3	325.2	-58.6	-26.4	-93.4	360.5	-9.53	-0.24	-85.5

5. Conclusions

Numerical analyses of the liquid tightness of the outer concrete tank in conditions following an emergency spillage were performed in three different ways. In the first method, as in the existing analysis method, the behavior of the tank was calculated based only on a steady state internal temperature. In the second, the variation of the internal temperature over time was considered and the structural behavior was calculated at various time steps from the beginning of the spillage to the steady state internal temperature distribution. In the third, not only the transient states of the

temperature but also the mechanical properties of the concrete depending on temperature and moisture content were taken into account in the analysis. With respect to estimating the liquid tightness, the following results were found through this study.

- The number of cracks with a width of more than 0.3 mm was greater in the analysis that considered the transient temperature states. At the beginning of the transient temperature state, the temperature gradient was steeper near the inside of the wall than for the steady state. The initially steeper gradient induces a larger number of cracks, and the cracks propagate until the temperature distribution reaches a steady state.
- The lateral displacement of the wall due to thermal contraction was larger in the analysis based on transient states of temperature. The larger deformation may also be due to the larger number of cracks in the second and third analysis cases.
- The results of the cracking and the deformation for the second and the third analysis cases were relatively similar to each other, compared to the difference between the first case and other cases.
- The results of the reinforcement stress for the three cases were very similar to one another. The stress level in tension was much higher than that in compression. The reinforcements located in the inner part of the wall bear almost the entire amount of the tension force because of concrete cracking, while the reinforcements and the concrete are subjected to compression force together in the outer part of the wall. This is the reason for the higher level of stress in the tension region.
- The average stress of the minimum compressive zones was the highest in the third analysis case, and the smallest in the second case. The size of the minimum compressive zone for the vertical stress was very similar to one another, and the size for the hoop stress became wider in the second and third cases.
- In engineering practice, the difference between the results obtained from the three different analysis cases is not meaningful, and the existing analysis method is still acceptable. However, if a more precise prediction for the behavior of the outer tank in the spillage is needed, it would be desirable to first consider the transient states of the temperature and second the mechanical properties of the concrete depending on the temperature and the moisture content.

Acknowledgment

This work was financially supported by the Samsung C&T Corporation. The authors are very grateful for the support.

This paper was written in the sabbatical year of the fifth author. The fifth author is grateful for the support of Myongji University.

References

ACI 373R-97 (1997), "Design and construction of circular prestressed concrete structures with circumferential tendons", *American Concrete Institute*, USA.

ADINA R&D, INC. (2011), *Theory and Modeling Guide- Volume I: ADINA*, ADINA Report ARD 11-8, 397-416.

Bamforth, P.B., Murray, W.T. and Browne, R.D. (1983), "The application of concrete at cryogenic

temperature to LNG tank design", *2nd International Conference on Cryogenic Concrete*, Amsterdam, Netherland.

Bathe, K.J., Walczak, J., Welch, A. and Mistry, N. (1989), "Nonlinear analysis of concrete structures," *Comput. Struct.*, **32**(3, 4), 563-590.

BS 7777 (1993), "Flat-bottomed, Vertical, Cylindrical storage tanks for low temperature service", *British Standards Institution*, UK.

BS 8110-1 (1997), "Structural use of concrete - Part I: code of practice for design and construction", *British Standards Institution*, UK.

Dahmani, L., Khenane, A. and Kaci S. (2007), "Behavior of the reinforced concrete at cryogenic temperatures", *Cryogenics*, 47(9-10), 517-525.

Gillard, M.N.T., Leslie, M.J. Vaughan, D.J. and Spencer, W.A. (2012), "Liquefied natural gas tank analysis: Cryogenic temperatures and seismic loading", *Proceedings of ICE-Engineering and Computational Mechanics*, 165(1), 49-56.

Gorla, R.S.R. (2010), "Rapid calculation procedure to determine the pressurizing period for stored cryogenic fluids", *Appl. Thermal Eng.*, **30**, 1997-2002.

Goto, Y. and Miura, T. (1978), "Mechanical properties of concrete at very low temperature", *Proceedings of 21st Japan Congress on Materials Research*, 157-159.

Goto, Y. and Miura, T. (1979), *Experimental Studies on Properties of Concrete Cooled to about Minus 160°C*, Technology Report (Tohoku University), **44**(2), 357-385.

Jeon, S.J. (2004), "Consistent Assessment for Liquid Tightness of LNG Storage Tank Subjected to Cryogenic Temperature-induced Forces", *J. Korean Soc. Civil Eng.*, **24**(1A), 203-210.

Jang, K.P., Sohn, J.K., and Kwon, S.H., (2013), "Prediction of Interfacial Cracking due to Differential Drying Shrinkage of Concrete in Precast Shell Pier Cap, "CMC-Computers, Materials and Continua, 38(3), 155-172.

Jeon, S.J., Jin, B.M. and Kim, Y.J. (2007), "Consistent thermal analysis procedure of LNG storage tank," *Struct. Eng. Mech.*, 25(2), 445-466.

Jo, S.D., Park, C.K, Jeong J.H., Lee, S.H. and Kwon, S.H. (2009), "A computational approach to estimating a lubricating layer in concrete pumping", *Comput. Mater. Continua*, **27**(3), 189-210.

Khatri D. and Anderson J.C. (1995), "Analysis of Reinforced Concrete Shear Wall Components Using the ADINA Nonlinear Concrete Model", *Comput. Struct.*, **56**(2, 3), 485-504.

Kogbara, R.B., Iyengar, S.R., Grasley, Z.C., Masad, E.A. and Zollinger, D.G. (2013), "A Review of Concrete Properties at Cryogenic Temperatures: Towards Direct LNG Containment", *Construct. Build. Mater.*, **47**, 760-770.

Krstulovic-Opara, N. (2007), "Liquefied Natural Gas Storage: Materials Behavior of Concrete at Cryogenic Temperatures", *ACI Mater. J.*, **104**(3), 297-306.

Kwon, S.H., Ferron R.P., Akkaya, Y. and Shah, S.P. (2007), "Cracking of Fiber-Reinforced Self-Compacting Concrete due to Restrained Shrinkage", *Int. J. Concrete Struct. Mater.*, **1**(1), 3-9.

Kwon, S.H. and Shah, S.P. (2008), "Prediction of Early –Age Cracking of Fiber-Reinforced Concrete due to Restrained Shrinkage", *ACI Mater. J.*, **105**(4), 381-389.

Lee, S.R. (2006), "Safety comparison of LNG tank designs with fault tree analysis," *23rd World Gas Conference*, Amsterdam.

Lee, Y., Choi, M.S., Yi, S.T. and Kim, J.K. (2009), "Experimental Study on the Convective Heat Transfer Coefficient of Early-Age Concrete", *Cement Concrete Compos.*, 31(1), 60-71.

Marshall, A.L. (1982), "Cryogenic Concrete", Cryogenics, **22**(11), 555-565.

Marechal, J.C. (1972), "Variation in the Modulus of Elasticity and Poisson's Ratio with Temperature," *ACI Special Publication 34: International Seminar on Concrete for Nuclear Reactor*, 495-503.

Miura, T. (1989), "The Properties of Concrete at Very Low Temperature", *Mater. Struct.*, **22**(130), 243-254.

Monfore, G.E. and Lentz, A.E. (1962), "Physical Properties of Concrete at Very Low Temperatures", *J. PCA R&D Labs*, 33-39.

Okada, T. and Iguro, M. (1978), "Bending behavior of prestressed concrete beams under low temperature", *J. Japan Prestressed Concrete Engineering Association*, 20th Special Issue for 8th FIP Congress, 17-35.

PCI Committee on Precast, Prestressed Concrete Storage Tanks (1987), "Recommended Practice for Precast Prestressed Concrete Circular Storage Tanks", *PCI J.*, **32**(4), 80-125.

prEN 265002 (2001), "Specification for the Design, Construction and Installation of Site Built, Vertical, Cylindrical, Flat-bottomed Steel Tanks for the Storage of Refrigerated, Liquefied Gases with Operating Temperature between -5 ℃ and -165℃," *CEN TC 265*.

prEN 14620 (2003), "Design and manufacture of site built, Vertical, Cylindrical, Flat-bottomed Steel Tanks for the Storage of Refrigerated, Liquefied Gases with Operating Temperature between -5 ℃ and -165℃," *CEN TC 265*.

Rötzer, J. and Douglas, H. (2006), "Liquid spill hazard investigated for LNG tanks", *Eng. Forum, LNG Journal*, October 2006, 32-33.

Rostasy, F.S. and Wiedemann, G. (1980), "Stress-strain-behavior of concrete at extremely low temperature", *Cement Concrete Res.*, **10**, 565-572.

Yamane, S., Kasami, H. and Okura, T. (1978), "Properties of concrete at very low temperatures", *ACI Special Publication 55: Douglas Mchenry International Symposium on Concrete and Concrete Structures*, 207-221.

CC